



## Utilizing the Drake Passage Time-series to understand variability and change in subpolar Southern Ocean pCO<sub>2</sub>

Amanda R. Fay<sup>1</sup>, Nicole S. Lovenduski<sup>2</sup>, Galen A. McKinley<sup>1</sup>, David R. Munro<sup>2</sup>, Colm Sweeney<sup>3-4</sup>, Alison R. Gray<sup>5</sup>, Peter Landschützer<sup>6</sup>, Britton Stephens<sup>7</sup>, Taro Takahashi<sup>1</sup>,  
5 Nancy Williams<sup>8</sup>

<sup>1</sup>Lamont Doherty Earth Observatory of Columbia University, New York, NY, USA

<sup>2</sup>Department of Atmospheric and Oceanic Sciences and Institute of Arctic and Alpine Research, University of Colorado, Boulder, CO, USA

10 <sup>3</sup>Cooperative Institutes for Research in Environmental Sciences, University of Colorado, Boulder, CO, USA

<sup>4</sup>NOAA Earth System Research Laboratory, Boulder, CO, USA

<sup>5</sup>School of Oceanography, University of Washington, Seattle, WA, USA

15 <sup>6</sup>Max Planck Institute for Meteorology, Hamburg, Germany

<sup>7</sup>National Center for Atmospheric Research (NCAR), Boulder, CO, USA

<sup>8</sup>College of Earth, Ocean, and Atmospheric Sciences, Oregon State University, Corvallis, OR, USA

### Abstract

20

The Southern Ocean is highly under-sampled for the purpose of assessing total carbon uptake and its variability. Since this region dominates the mean global ocean sink for anthropogenic carbon, understanding temporal change is critical. Underway measurements of pCO<sub>2</sub> collected as part of the Drake Passage Time-series (DPT) program that began in 2002 inform our understanding of seasonally changing  
25 air-sea gradients in pCO<sub>2</sub>, and by inference the carbon flux in this region. Here, we utilize all available pCO<sub>2</sub> observations collected in the subpolar Southern Ocean to evaluate how the seasonal cycle, interannual variability, and long-term trends in surface ocean pCO<sub>2</sub> in the Drake Passage region compare to that of the broader subpolar Southern Ocean. Our results indicate that the Drake Passage is representative of the broader region in both seasonality and long term pCO<sub>2</sub> trends shown through the agreement of timing  
30 and amplitude of seasonal cycles as well as trend magnitudes. The high temporal density of sampling by the DPT is critical to constraining estimates of the seasonal cycle of surface pCO<sub>2</sub> in this region, as winter data remain sparse in areas outside of the Drake Passage. From 2002-2015, data show that carbon uptake has strengthened with surface ocean pCO<sub>2</sub> trends less than the global atmospheric trend in the Drake Passage and the broader subpolar Southern Ocean. Analysis of spatial correlation shows Drake Passage  
35 pCO<sub>2</sub> to be representative of pCO<sub>2</sub> and its variability up to several hundred kilometers upstream of the region. We also compare DPT data from 2016 and early 2017 to contemporaneous pCO<sub>2</sub> estimates from



autonomous biogeochemical floats deployed as part of the Southern Ocean Carbon and Climate  
Observations and Modeling project (SOCCOM) so as to highlight the opportunity for evaluating data  
collected on autonomous observational platforms. Though SOCCOM floats sparsely sample the Drake  
40 Passage region for 2016-2017, their  $p\text{CO}_2$  estimates typically fall within the range of underway  
observations. Going forward, continuation of the Drake Passage Time-series will reduce uncertainties in  
Southern Ocean carbon uptake seasonality, variability, and trends, and provide an invaluable independent  
dataset for post-deployment quality control of sensors on autonomous floats. Together, these datasets will  
vastly increase our ability to monitor change in the ocean carbon sink.

45

### 1. Introduction

The Southern Ocean plays a disproportionately large role in the global carbon cycle. Over the past few  
decades, the ocean has absorbed approximately 26% of the carbon dioxide ( $\text{CO}_2$ ) emissions from fossil fuel  
burning and land use change [Le Quéré et al., 2016, 2017], and since the preindustrial era, the ocean has  
50 been the primary sink for anthropogenic emissions [McKinley et al. 2017; Ciais et al., 2013]. The Southern  
Ocean (south of  $30^\circ\text{S}$ ) accounts for almost half of the total oceanic sink of anthropogenic  $\text{CO}_2$  [Frölicher et  
al. 2015; Gruber et al. 2009; Takahashi et al. 2009]. Though the importance of this region is widely  
understood, the scarcity of surface ocean carbon-related observations in the Southern Ocean hampers our  
ability to understand how this anthropogenic  $\text{CO}_2$  uptake occurs against the background of natural  
55 variability.

Observations and models suggest large variability in the strength of Southern Ocean  $\text{CO}_2$  uptake on decadal  
timescales. Several studies have reported a slow-down or reduction in the efficiency of Southern Ocean  
 $\text{CO}_2$  uptake from the 1980's to the early 2000's [Le Quéré et al. 2007; Lovenduski et al. 2008; Metzl 2009;  
60 Takahashi et al. 2012; Fay and McKinley, 2013; Lovenduski et al. 2015; Landschützer et al. 2014a, 2015a],  
followed by a substantial strengthening of the Southern Ocean  $\text{CO}_2$  sink since 2002 [Fay and McKinley,  
2013; Fay et al. 2014; Landschützer et al. 2015a; Munro et al. 2015a; Xue et al. 2015]. Continued  
observational sampling efforts and coordination are required for quantifying and understanding decadal  
changes in this important  $\text{CO}_2$  sink region.



65

Initiated in 2002 and continuing to present, the Drake Passage Time-series (DPT) is unique among Southern Ocean research programs in both its spatial and temporal coverage. High-frequency underway observations of the surface ocean partial pressure of CO<sub>2</sub> (pCO<sub>2</sub>) are collected on the Antarctic Research and Supply Vessel *Laurence M. Gould* on up to 20 crossings per year from the southern tip of South

70

America to the Antarctic Peninsula, spanning the Antarctic Circumpolar Current (ACC) and its associated Antarctic Polar Front [Munro et al. 2015a, 2015b]. The DPT is also notable for sampling surface ocean pCO<sub>2</sub> during the austral winter in all years from 2002 to present, providing valuable information about the full seasonal cycle of pCO<sub>2</sub> in the poorly sampled Southern Ocean. Other ships have contributed observations in the Drake Passage region including the *Polarstern* and the *Nathaniel B. Palmer*, however

75

none have the consistent temporal coverage as provided by the DPT.

The surface ocean pCO<sub>2</sub> observations from the DPT have provided the foundation for larger data sets, which have been extensively used to examine variability and trends in CO<sub>2</sub> uptake in the broader Southern Ocean [Fay and McKinley, 2013; Fay et al. 2014; Majkut et al. 2014; Landschützer et al. 2014b, 2015b;

80

Rödenbeck et al. 2015]. In many of these studies, interpolated estimates of Southern Ocean pCO<sub>2</sub> are used in conjunction with measurements of atmospheric pCO<sub>2</sub> to estimate variability and trends in the air-sea pCO<sub>2</sub> gradient and when combined with wind speed, air-sea CO<sub>2</sub> fluxes.

85

The physical oceanography of the Drake Passage region is unique in the Southern Ocean. Here, the strong flow of the zonally unbounded ACC is funneled through a narrow constriction (~800 km), making it an ideal location for sampling across the entire ACC system over a relatively short distance [Sprintall et al. 2012]. At the same time, the unique nature of the circulation could potentially reduce the degree to which the Drake Passage region is representative of the broader region. The DPT program takes advantage of frequent *Gould* crossings to conduct physical and biogeochemical sampling of the ACC system. Thus,

90

before conclusions can be drawn about large-scale Southern Ocean carbon uptake and its variability using data from the DPT, it is important to document how pCO<sub>2</sub> in this particular region compares with pCO<sub>2</sub> measured elsewhere in the subpolar Southern Ocean. In this study, we utilize all available pCO<sub>2</sub>



95 observations collected in the subpolar Southern Ocean to evaluate how the seasonal cycle, interannual  
variability, and long-term trends in surface ocean  $p\text{CO}_2$  in the Drake Passage region compare to that of the  
broader subpolar Southern Ocean. Further, we highlight the opportunity for quality control of autonomous  
observational platforms passing through the Drake Passage utilizing the underway  $p\text{CO}_2$  measurements  
from the DPT.

## 2. Data

100 This study uses several observational datasets and data products of surface ocean  $p\text{CO}_2$  in the Southern  
Ocean: measurements from the Surface Ocean  $\text{CO}_2$  Atlas (SOCAT), which includes underway  
measurements from the DPT, interpolated estimates of the SOCAT data using a self-organizing map feed-  
forward neural network (SOM-FFN) approach, and calculated  $p\text{CO}_2$  estimates from biogeochemical Argo  
floats. While the SOCAT database reports the fugacity of carbon dioxide ( $f\text{CO}_2$ ), for our analysis we  
105 consider datasets reporting  $p\text{CO}_2$  and  $f\text{CO}_2$  to be interchangeable which is an acceptable assumption for  
surface ocean observations as  $\text{CO}_2$  behaves closely to an ideal gas. Globally, the difference between these  
parameters is less than  $2\mu\text{atm}$ , which is roughly the reported uncertainty of shipboard observations of  $p\text{CO}_2$   
and well within the uncertainty of the observation-based  $p\text{CO}_2$  estimates. Below, we describe each of these  
data sources in turn.

110

### 2.1 The Drake Passage Time-series (DPT)

A unique dataset of ongoing year-round observations beginning in 2002 is available from the Drake  
Passage Time-series (DPT), providing an unprecedented opportunity to characterize the mean and time  
varying state of the Drake Passage and the surrounding waters using direct observations. This dataset  
115 includes high frequency underway observations of surface ocean  $p\text{CO}_2$ , in addition to other physical and  
biogeochemical variables including discrete measurements of total  $\text{CO}_2$  ( $\text{TCO}_2$ ) which, together with  $p\text{CO}_2$   
and nutrients, allow a complete understanding of the carbonate system in the DPT. Analytical methods used  
to measure  $p\text{CO}_2$ , as well as the methods used to calculate nutrient and carbonate parameters are described  
in detail by Munro et al. [2015a, 2015b].

120



## 2.2 Surface Ocean CO<sub>2</sub> Atlas (SOCAT)

SOCAT is a global surface ocean carbon dataset of fCO<sub>2</sub> values (pCO<sub>2</sub> corrected for the non-ideal behavior of CO<sub>2</sub>) starting in 1957 [Sabine et al. 2013; Pfeil et al. 2013]. In this study we utilize version 4 of this product (SOCATv4), which includes roughly 18.5 million observations globally [Bakker et al., 2016], including 737,000 observations contributed from the DPT. Despite the large number of observations available in the Southern Ocean, data is spatially and temporally concentrated, with strong seasonal biases. Most data is collected during reoccupations of supply routes to Antarctic bases or on repeat hydrographic lines, which leaves large bands of the Southern Ocean completely unsampled [Bakker et al. 2016].

## 2.3 Self-organizing Map Feed-forward Network Product (SOM-FFN)

Landschützer et al. [2014b] use a two-step neural network approach to extrapolate the monthly gridded SOCAT product in space and time. This results in reconstructed basin-wide monthly maps of the sea surface pCO<sub>2</sub> at a resolution of 1° × 1° [Landschützer et al. 2017]. Air-sea CO<sub>2</sub> flux maps are then computed using a standard gas exchange parameterization and high-resolution wind speeds. The neural network estimate is described and substantially validated in past publications [Landschützer et al. 2014, 2015a, 2016] and it was shown that the estimates fit observed pCO<sub>2</sub> data in the Southern Ocean with a root mean square error (RMSE) of about 20 µatm and with almost no bias [Landschützer et al. 2015a, supplementary material].

The SOM-FFN product used in this analysis is created from SOCATv4. Additionally, we generated an alternative SOM-FFN product (SOM-FFN-noDP) using the same methodological setup but excluding the pCO<sub>2</sub> data collected in the Drake Passage region for years 2002-2015, which represents the years of the DPT program.

## 2.4 SOCCOM Floats

The Southern Ocean Carbon and Climate Observations and Modeling (SOCCOM) project (<http://socom.princeton.edu>) aims to deploy approximately 200 biogeochemical profiling floats over a five-year period (2015 to 2020) in an effort to fill observational gaps in the Southern Ocean. In total, over



90 floats carrying some combination of additional biogeochemical sensors (i.e., pH, nitrate, oxygen,  
150 fluorescence, and backscattering) have been collecting data since April 2014 [Johnson & Claustre, 2016].  
With the float's capability to measure pH and utilization of existing algorithms for predicting total  
alkalinity, pCO<sub>2</sub> can be calculated from the collected observations [Williams et al. 2017] and compared to  
underway observations.

155 The uncertainty range for these calculated pCO<sub>2</sub> values is estimated to be ±11 µatm and results from  
various components of the calculation procedure [Williams et al. 2017]. pCO<sub>2</sub> estimates from autonomous  
floats such as the SOCCOM floats have not been included in the SOCAT database because they do not  
report original surface water CO<sub>2</sub> data. For consistency, we maintain this separation in our analysis and  
limit our study of SOCCOM floats to direct comparisons to DPT values in Section 5.

160

### 3. Methods

The SOCATv4 database sub-sampled from 2002-2015 is considered here to match the years of overlap  
with DPT observations, which began in 2002. The SOCAT dataset is then subsampled to include only  
observations with reported salinity values in the 33.5 - 34.5 psu range and a distance-to-land value greater  
165 or equal to 50 km. This step restricts our analysis to open-ocean observations, since coastal observations  
report lower salinity values, which correspond to low pCO<sub>2</sub> values, due to the influence of fresh water and  
ice melt. SOCCOM float files were downloaded on 26 September 2017 and reported pCO<sub>2</sub> values are an  
average of all data collected in the top 20m of water to remain consistent with previous SOCCOM float  
analysis (Williams et al. 2017).

170

The Southern Ocean region of interest is the Southern Ocean Subpolar Seasonally Stratified (SPSS) biome  
as defined in Fay and McKinley [2014] (Figure 1) as it encompasses the Drake Passage. We further define  
the Drake Passage region as the portion of the Southern Ocean SPSS biome bounded by 55°W and 70°W  
lines of longitude (Figure 1). This is similar to the region analyzed in Munro et al [2015a] however it  
175 extends the region of interest to the northern and southern extents of the SPSS biome.



Alternate definitions of the larger Southern Ocean region of interest were considered during our analysis, including a subdivision of the SPSS into a Northern SPSS and Southern SPSS, with the boundary defined by the location of the mean position in the Antarctic Polar Front [Freeman and Lovenduski 2016; Freeman  
180 et al. 2016; Munro et al. 2015b], as well as the Polar Antarctic Zone [Williams et al. 2017] (Supplementary Figures 1-3). The overall conclusions remain largely unchanged when using these alternate regional definitions.

In order to compare the seasonal cycle and long-term trends in the Drake Passage with the broader SPSS  
185 biome, we analyze surface ocean  $p\text{CO}_2$  from 3 subsets of the SOCAT database: SOCAT-all which includes all available SOCATv4 data from 2002-2015 in the SPSS biome, SOCAT-DP which includes SOCATv4 data within the longitudinally-defined Drake Passage region (Figure 1, with 62% of data this collected onboard the *R/V Gould*), and SOCAT-noDP which excludes any data within the longitudinally-defined Drake Passage region of the SPSS biome. All datasets are first averaged to monthly,  $1^\circ \times 1^\circ$  resolution.  
190 Monthly means are then calculated for the SPSS biome by first removing the background mean climatological value of  $p\text{CO}_2$  at each  $1^\circ \times 1^\circ$  location [Landschützer et al. 2014a] to aid in accounting for the potential of spatial aliasing in the sparsely sampled Southern Ocean [Fay and McKinley, 2013].

Biome-scale monthly means are compared and used to calculate seasonal cycles and trends. Seasonal  
195 cycles are calculated by first removing a  $1.95 \mu\text{atm yr}^{-1}$  trend to account for increasing atmospheric  $\text{CO}_2$  during the 2002-2015 period [Dlugokencky et al. 2015]. Seasonal uncertainties (Figure 2) are estimated as 1 standard error from the mean of all available biome mean values for a given month. This is a conservative estimate of the uncertainty in any given month because of inconsistent annual coverage and spatial undersampling biases. Reported trends are calculated by fitting a single harmonic and linear trend to the  
200 biome-scale monthly means as done in Fay and McKinley [2013]. Trends are not statistically different if the calculated mean seasonal cycle is removed instead of the choice to fit a harmonic to the data. Seasonal trends are calculated with a simple linear fit to the seasonal monthly means.

#### 4. Results and Discussion



#### 205 4.1 Seasonal cycle

The mean seasonal cycle of  $p\text{CO}_2$  in the Southern Ocean SPSS biome for the 3 SOCAT datasets and the full SOM-FFN estimate indicate broad agreement (Figure 2). Here, surface ocean  $p\text{CO}_2$  levels reach a maximum in austral winter (June to August), when deep mixing delivers carbon-rich water to the surface, and a minimum in austral summer (December to February), when biological production draws down the

210 inorganic carbon from the surface [Takahashi 2009]. Temperature also plays a role in modulating the  $p\text{CO}_2$  seasonal cycle in the Southern Ocean. Winter cooling drives  $p\text{CO}_2$  lower at the same time as deep winter mixing elevates surface carbon levels. During the summer, warming temperatures raise  $p\text{CO}_2$  while biological utilization of carbon drives surface  $p\text{CO}_2$  levels lower [Munro et al. 2015b]. The average amplitude of the detrended seasonal cycle of  $p\text{CO}_2$  (max-min) is  $23 \mu\text{atm}$  (Figure 2), smaller than the high

215 latitude oceans in the Northern Hemisphere [Takahashi et al. 2002, 2009; Landschützer et al. 2015b]. The small amplitude of the  $p\text{CO}_2$  seasonal cycle in this region is due to the similar magnitude and opposite phasing of temperature and carbon supply/utilization effects. In all months, surface ocean  $p\text{CO}_2$  levels in the Southern Ocean SPSS are below atmospheric which ranges from an annual mean of  $372 \mu\text{atm}$  in 2002 to  $399 \mu\text{atm}$  in 2015, indicating that this region has been a persistent  $\text{CO}_2$  sink over the period of analysis

220 [Dlugokencky & Tans, 2017].

Figure 2 also shows the uncertainty of the seasonal mean, with shading representing 1 standard error from the monthly mean for each dataset. Uncertainty estimates vary for each month of the seasonal cycle with a minimum uncertainty of  $1.1 \mu\text{atm}$  (June, SOCAT-DP) to a maximum of  $5 \mu\text{atm}$  (July, SOCAT-DP).

225 Seasonal cycles are consistent when analyzing the PAZ region (Supp Figure 2), however the SOCAT-DP seasonal cycle exhibits two maxima possibly due to the omission of the southern area of the Drake Passage. The June peak in SOCAT-noDP also remains when considering the PAZ region.

Figure 3 indicates how inconsistent Southern Ocean  $p\text{CO}_2$  data density is in space and time. Even given the

230 sampling efforts of the DPT, repeated occupations of SR03 south of Australia [Shadwick et al. 2015], along the Prime Meridian [Hoppema et al. 2009; Van Heuven et al. 2011], and in the southwestern Indian sector [Metzl et al. 1999; Lo Monaco et al. 2005, 2010; Metzl, 2009], consistent monthly observations are not



always possible. Specifically, during austral winter, data availability outside of the Drake Passage region is extremely limited due to the few ships operating in winter and the difficult conditions that the wintertime  
235 Southern Ocean presents to data collection efforts (Figure 3b).

The average seasonal cycles of the 3 SOCAT datasets are quite similar, with few statistically-significant differences given the uncertainty bounds. SOCAT data from the Drake Passage region (SOCAT-DP) exhibits relatively large estimated uncertainty (average for all months = 2.31  $\mu\text{atm}$ ), despite the high  
240 temporal coverage and smaller region considered. This indicates that large interannual variability is inherent to the Drake Passage region, especially in the well-observed austral summer months. Despite data being much more regularly collected in this region than in the rest of the Southern Ocean (Figure 3), there are still months of quite limited observations, specifically July and August (Figure 2). SOCAT-all has monthly uncertainties averaging 1.8  $\mu\text{atm}$  with the largest uncertainties in January and July. Data  
245 availability for SOCAT-all is consistent for much of the year, with most months having observations in at least 12 of the 14 years considered in this analysis (Figure 2). The exceptions are July and August that have data from only 7 and 9 years, respectively.

The SOCAT-noDP seasonal cycle is similar to that of the other datasets but deviates in the austral  
250 fall/winter, specifically May and June. In winter, SOCAT-noDP suggests higher  $\text{pCO}_2$  than SOCAT-DP or SOCAT-all, though the limited data in June and July must be considered when drawing conclusions from this difference (Figure 2, 3b). With June and July data available for fewer than 4 of the 14 years covered in the analysis it is possible that the peak shown here could be biased by the few years included, specifically for the month of June. In contrast, SOCAT-DP and SOCAT-all have data for nearly all of the years  
255 considered in these months. The data that is available during May and June in SOCAT-noDP is from regions downstream of the Drake Passage (Figure 3b) where we expect data to be less similar to that collected in the Drake Passage.

Similar comparisons are seen in the PAZ region (Supp Figure 2). The double maxima seasonal cycle  
260 exhibited by the SOCAT-DP dataset is likely caused by the smaller region which eliminates data south of



the front (Supp Figure 1) which would cause PAZ region averages to be greater than those shown for the DP region of the SPSS.

Overall, given available data, the seasonal cycles are statistically indistinguishable for data collected inside  
265 and outside of the Drake Passage region, for all months with at least 4 years of observations (Figure 2).  
This indicates that the Drake Passage seasonal cycle is representative of the broader SPSS biome  
seasonality, based on the available observations to date, but increased observations outside of the Drake  
Passage during May and June would provide a more robust comparison. Additionally, the seasonal cycles  
from all 3 SOCAT datasets closely resemble the smoothed seasonality of the interpolated SOM-FFN  
270 product in the SPSS biome (Figure 2). However, sparse sampling outside of the Drake Passage during  
winter months leads to this estimated seasonal cycle likely being driven by Drake Passage data. Enhanced  
wintertime data collection, especially in regions outside of the Drake Passage, is required to better constrain  
the full seasonal cycle of surface ocean pCO<sub>2</sub> in the Southern Ocean SPSS.

#### 275 4.2 Interannual variability

The high resolution of the time-series data in the Drake Passage allows for close examination of temporal  
variability in pCO<sub>2</sub> with relatively low uncertainty [Munro et al. 2015a]. We investigate the interannual  
variability in Drake Passage pCO<sub>2</sub> in Figure 4a, where deseasonalized and detrended anomalies [Fay and  
McKinley, 2013] from the SOCAT-DP dataset are shown in gray, with the black line representing these  
280 anomalies smoothed with a 12-month running mean. Over the 2002-2015 period, the variance in pCO<sub>2</sub>  
anomalies is 60 μatm<sup>2</sup>. Monthly anomalies are as large as ±25μatm, and 12-month smoothed anomalies as  
large as ±8μatm in this dataset.

A model-based study by Lovenduski et al. [2015] find interannual variability in pCO<sub>2</sub> to be low in the  
285 Drake Passage compared to other Southern Ocean regions. However, we find that detrended and  
deseasonalized anomalies from SOCAT-noDP and SOCAT-DP have comparable variances (56 μatm<sup>2</sup> and  
60 μatm<sup>2</sup>). This result, however, is likely strongly affected by the previously-discussed seasonal data gaps  
outside of the DP region. Conducting a similar analysis of the reported SOCAT sea surface temperature



(SST) values does find the variance for SOCAT-DP to be significantly lower than SOCAT-noDP ( $0.92^{\circ}\text{C}^2$  and  $2.73^{\circ}\text{C}^2$  respectively). As the same sampling issues exist for SST as for  $\text{pCO}_2$  in SOCAT, an alternate method to address this issue is needed to resolve these conflicting results.

The SOM-FFN data product does offer complete seasonal and regional coverage, and thus the comparison of variance in Drake Passage to all the Southern Ocean can be made in this context. Results for SOM-FFN are different from both the SOCAT findings above and the results of Lovenduski et al. [2015]. For the SPSS biome area of SOM-FFN  $\text{pCO}_2$ , the variance of detrended and deseasonalized anomalies is significantly higher within the Drake Passage region than outside of the region ( $10.4 \mu\text{atm}^2$  and  $4.4 \mu\text{atm}^2$ , respectively). It should be noted that variances are significantly lower for the SOM-FFN because of its interpolation. We are left without a clear picture as to whether Drake Passage is more or less variable in  $\text{pCO}_2$  than the rest of the Southern Ocean SPSS. This conundrum is clearly due to the lack of data availability, particularly outside the Drake Passage during winter months (Figure 3b).

Given the lack of data, the degree to which Drake Passage represents the interannual variability of the Southern Ocean SPSS can only be considered in the context of the SOM-FFN data product. To produce independent estimates of correlations between Drake Passage and other points, we use a version of the SOM-FFN product created without the inclusion of any observations in our defined Drake Passage region (SOM-FFN-noDP, Figure 4b), and assess correlations to SOCAT data within the Drake Passage. Anomalies have been detrended and deseasonalized, and grayed areas indicate that the correlation is not significant at the 95% confidence level (Figure 4b). The strongest positive correlations are within Drake Passage, upstream of the Drake Passage into the central Pacific SPSS, and in the Indian Ocean sector of the SPSS biome (Figure 4b). Weaker positive correlations are found in the western Pacific SPSS, as well as a few areas in the Atlantic sector of the SPSS. No regions of widespread strong negative correlations are observed in the SPSS biome. Surface ocean  $\text{pCO}_2$  in the central and eastern Pacific regions, upstream of the Drake Passage, are highly correlated on interannual timescales with the  $\text{pCO}_2$  measured in the Drake Passage. This is consistent with the analysis of Munro et al. [2015b] who estimate the footprint of the Drake Passage extending upstream into the eastern Pacific sector of the ACC.



#### 4.3 Trends, 2002-2015

Trends for all data (annual), as well as summer and winter, are estimated from the three SOCAT datasets,  
320 the SOM-FFN data product, and the SOM-FFN product subsampled as SOCAT-DP, in all cases following  
the approach of Fay & McKinley [2013]. Similar to the climatological pCO<sub>2</sub> seasonal cycle, annual trends  
for the 3 SOCAT datasets are indistinguishable given the 68% confidence intervals (Figure 5).

All annual trends are less than the 2002-2015 atmospheric pCO<sub>2</sub> trend of 1.95  $\mu\text{atm yr}^{-1}$  [Dlugokencky et al.  
325 2015], indicating that the Southern Ocean has been a growing sink for atmospheric carbon over 2002-2015  
(Figure 5, far left). Comparing the different estimates, SOCAT-DP (gray bar) has an annual trend just  
slightly below that of the full SOM-FFN, however with a much greater uncertainty. The annual trend from  
the SOCAT-all dataset (blue) is nearly identical to the SOCAT-DP trend in both mean and uncertainty.  
These are not statistically different from the SOCAT-noDP or the SOM-FFN. SOCAT-noDP yields the  
330 largest annual trend, but falls well below the atmospheric trend and remains indistinguishable from all the  
other datasets considered given the 1 $\sigma$  uncertainty bounds.

Sampling the SOM-FFN data product as the SOCAT-DP dataset is one way to estimate the impact of the  
available data coverage in the Drake Passage region as compared to the hypothetical situation of perfect  
335 data coverage in the SPSS biome. Sampling lowers the trend, making it significantly smaller than the full  
SOM-FFN trend. This reduction leads to an annual trend very similar to that of SOCAT-DP and SOCAT-  
all. This conclusion emphasizes the need for increased observations around the Southern Ocean as it  
implies we are not accurately capturing the theoretical trend in this region with the available data.

340 These comparisons are largely maintained for summer and winter trends (Figure 5, center and right).  
Uncertainty increases when considering seasonal trends due to reduced data quantity. All trends are  
statistically indistinguishable for summer months. For winter, SOCAT-noDP is not shown because unlike  
SOCAT-all and SOCAT-DP, not all years have available data during this season (Figure 2). Overall, winter  
trends are slightly higher than summer trends, but given the uncertainties, winter and summer trends are



345 only clearly distinguishable for the full SOM-FFN product, where the winter trend is nearly  $0.45 \mu\text{atm yr}^{-1}$   
higher than the summer trend. For summer and winter trends, the full and subsampled SOM-FFN products  
have trends that are indistinguishable within each season. Winter trends have larger differences and larger  
uncertainties, consistent with reduced data availability.

350 A further investigation of trends from the full SOM-FFN product and that of the SOM-FFN-noDP product  
for the entire Southern Ocean south of  $35^{\circ}\text{S}$  for years 2002-2015 indicates a steadily increasing carbon  
uptake by the ocean (Figure 6). If the Drake Passage data is omitted during the creation of the product  
(SOM-FFN-noDP), flux trends are unchanged (Figure 6a). However, the mean difference between these  
two products is a consistently lower estimate of the mean Southern Ocean  $\text{pCO}_2$  (Figure 6b). Both  
355 estimates illustrate that for 2002-2015, the Southern Ocean was an important sink of carbon dioxide. The  
comparison also shows that the mean  $\text{pCO}_2$  of the SOM-FFN product for the Southern Ocean is impacted  
by the inclusion of the Drake Passage data as shown by the offset between the lines in Figure 6.

##### **5. DPT as a $\text{pCO}_2$ evaluation point for biogeochemical profiling floats**

360 Starting in late 2014, autonomous biogeochemical profiling floats have been deployed as part of the  
SOCCOM project, and as of summer 2017, several floats had traveled through or were approaching the  
Drake Passage region (Figure 7b). These floats offer a new opportunity to complement our oceanographic  
understanding that has been developed primarily with traditional shipboard observations. Floats provide  
more frequent observations, regardless of weather or sea conditions. With satellite relays, float data can be  
365 made available in near-real time. However, as will be discussed in more detail, there are limitations of float  
observations (i.e. instrument drift, high uncertainty levels) that could potentially be addressed by taking  
advantage of the complementary strengths of the Drake Passage Time-series dataset. As the floats provide  
autonomous observations covering existing spatial and temporal gaps throughout the Southern Ocean and  
ship-based systems provide high density observations at considerably higher accuracy ( $\pm 11 \mu\text{atm}$  for floats  
370 compared to  $\pm 2 \mu\text{atm}$  for ships), there is great potential for these two observational platforms to work in  
concert to provide a whole Southern Ocean carbon observing system.



Here, underway DPT  $p\text{CO}_2$  data for 2016 and 2017 are used for comparison to SOCCOM floats. This is instead of the SOCATv4 because these data are not available after 2015. For March 2002-June 2017, 375 underway Drake Passage Time-series  $p\text{CO}_2$  data in the SPSS biome has a large range, often spanning over 100  $\mu\text{atm}$  each month (Figure 7a).  $p\text{CO}_2$  from all floats east of  $90^\circ\text{W}$  and west of  $55^\circ\text{W}$  (Figure 7b) are also plotted on the time-series (Figure 7a,c) with their calculated  $p\text{CO}_2$  value averaged from all depths  $<20\text{m}$ . Float-based  $p\text{CO}_2$  estimates mostly fall within the range of the direct underway  $p\text{CO}_2$  observations, however anomalies do exist. Float estimates in June and July 2017 (Figure 7c) report higher  $p\text{CO}_2$  values 380 than nearby DPT observations, however a lack of cruise data during this specific time limits direct comparisons. Overall, the range of the shipboard observations is far larger than the range of estimated  $p\text{CO}_2$  from the floats in most cases. This is likely due to the fact that shipboard observations regularly span across the width of the Drake Passage where decorrelation length scales are relatively short [Eveleth et al. 2017], while the floats sample along the ACC path. Despite the difference shown in this region, the 385 agreement of these few floats with the underway data is very encouraging (Figure 7a,c). As the floats offer autonomous, frequent observations and the ship offers data of the highest-quality, it is ideal for these two platforms to work in partnership.

A direct comparison between DPT data and SOCCOM floats indicates more precisely this potential (Figure 390 8). As of September 2017, six floats surfaced near DPT observations within a window of 75 km, 3 consecutive days, and have a reported SST within  $0.3^\circ\text{C}$  of each other (Figure 8a). This window is consistent with the crossover criteria used by the SOCAT community to quality control shipboard data [Pfeil et al. 2013; Olsen et al. 2013]. Figure 8a shows locations of the floats and the nearby DPT observations that fit this crossover window. As DPT offers high frequency observations, all available 395 measurements over the 3-day window are shown (Figure 8b). Also indicated are DPT observations that crossover within a 50km and 2-day window and 25km and 1-day window, both also with the  $0.3^\circ\text{C}$  SST criteria as well, for completeness (Figure 8b, black 'x' and boxes). A comparison of the calculated  $p\text{CO}_2$  from the floats and observed DPT  $p\text{CO}_2$  reveals a broad correspondence (passing through the 1:1 line) in all 400 measurements (Figure 8b shading). While all crossover floats do intersect the 1:1 line given their stated



uncertainties, these comparisons reveal the large range of pCO<sub>2</sub> captured by high-frequency shipboard measurements in a relatively small region and illustrates that this range cannot be fully captured by floats surfacing only once every 10 days. Further investigation of crossovers in the entire Southern Ocean region is warranted. While the DPT provides the most likely occurrence for this, other regions with frequent ship traffic could provide additional comparisons.

While autonomous biogeochemical floats can sample the larger Southern Ocean across all seasons, float sensor calibrations must be corrected initially after deployment by reference to deep (near 1500 m) pH values, which are estimated from multiple linear regression equations fitted to high quality, spectrophotometric pH observations made on repeat hydrography cruises [Williams et al., 2016; 2017; Johnson et al., 2016; 2017]. In addition, empirical algorithms for alkalinity must be used to estimate pCO<sub>2</sub> from float-based pH [Carter et al. 2016; Williams et al. 2016]. A thorough analysis of all sources of uncertainty estimated the total uncertainty in float-based pCO<sub>2</sub> to be as high as 11 μatm, although crossover comparisons with underway ship data collected close to the first float profile found a mean difference of only 3.7 μatm [Williams et al. 2017]. However, it is expected that the sensors will drift or require adjustments during their 4-5 year lifespan. Ship-based programs like the DPT should be utilized for post-deployment quality control assessments or data quality checks, both with the underway pCO<sub>2</sub> data from the surface (as shown in Figure 8), and more thoroughly if hydrocast observations were planned to occur in the vicinity of a passing biogeochemical float. Such coordinated efforts would advance monitoring of the carbon cycle in the Southern Ocean.

## 6. Conclusions

The Drake Passage Time-series illustrates the large variability of surface ocean pCO<sub>2</sub>, and exemplifies the value of sustained observations in understanding changing ocean carbon uptake in the Southern Ocean. This is the only location where carbon measurements throughout the entire annual cycle in the subpolar Southern Ocean have been made regularly over the past two decades. With this complete coverage we find seasonal amplitudes in the SPSS to be smaller than subpolar regions in the Northern Hemisphere, and controlled by a combination of temperature and deep water mixing effects. Uncertainties in the seasonality



remain considerable given the dynamic nature of this region and the short time-series considered.

430 Specifically, a lack of winter data in all years limits the conclusions for differences between the Drake Passage and the larger SPSS biome where we see a discrepancy in the timing of the winter maxima. These findings can direct specific goals for future observations. Specifically, insufficient wintertime data in regions outside of the Drake Passage limits our assessment of how representative Drake Passage data is of the larger region.

435

The magnitude of interannual variability is comparable for SOCAT pCO<sub>2</sub> data within and outside of the Drake Passage region of the SPSS biome, a finding that conflicts with results from previous modeling and analysis of the SOM-FFN product. A clear idea of whether the Drake Passage is more or less variable in pCO<sub>2</sub> will require increased data, particularly during the austral winter outside of the Drake Passage. Given  
440 these data restrictions, representativity of the larger SPSS biome is also investigated using the SOM-FFN product. Within this gap-filled data product, monthly anomalies in the Drake Passage region are representative of broad swaths of the Southern Ocean, specifically regions upstream of the Drake Passage, but also regions in the Indian Ocean sector of the Southern Ocean. Consistent with this finding, estimates of long-term trends do not change substantially if observations in the Drake Passage are removed from the  
445 SOM-FFN analysis. Across approaches to data analysis, trends in annual oceanic pCO<sub>2</sub> trends for 2002-2015 are less than the atmospheric pCO<sub>2</sub> trend, confirming previous findings that the Southern Ocean has been a growing sink for atmospheric carbon since 2002.

Comparisons between underway DPT and SOCCOM float measurements show general agreement over the  
450 Drake Passage and a fine-scale crossover investigation demonstrates their correspondence given uncertainty ranges for SOCCOM float pCO<sub>2</sub> estimates. Employing the high-temporal measurements of the DPT and frequent hydrocasts as comparisons could aid in reducing the uncertainty on the float pCO<sub>2</sub> measurements by helping to identify problematic float sensors. Coordinated monitoring efforts that combine a well-calibrated array of autonomous biogeochemical floats with a robust ship-based  
455 observational network will improve and expand monitoring of the carbon cycle in the Southern Ocean in the future.



460 **Acknowledgements.** We are grateful for funding from NSF (PLR-1543457, OCE-1558225, OCE-  
 1155240), NOAA (NA12OAR4310058), and NASA (NNX17AK19G). NCAR is sponsored by the  
 National Science Foundation. We acknowledge support from the Space Science and Engineering Center of  
 University of Wisconsin – Madison and Columbia University. The authors are especially grateful for the  
 efforts of the marine and science support teams of the ARSV Laurence M. Gould, particularly Timothy  
 465 Newberger, Kevin Pedigo, Bruce Felix, and Andy Nunn. Underway DPT measurements presented in this  
 manuscript are archived at NOAA's National Centers for Environmental Information  
 ([https://www.nodc.noaa.gov/ocads/oceans/VOS\\_Program/LM\\_gould.html](https://www.nodc.noaa.gov/ocads/oceans/VOS_Program/LM_gould.html)). The Surface Ocean CO<sub>2</sub> Atlas  
 (SOCAT) is an international effort, supported by the International Ocean Carbon Coordination Project  
 (IOCCP), the Surface Ocean Lower Atmosphere Study (SOLAS), and the Integrated Marine  
 470 Biogeochemistry and Ecosystem Research program (IMBER), to deliver a uniformly quality-controlled  
 surface ocean CO<sub>2</sub> database. The many researchers and funding agencies responsible for the collection of  
 data and quality control are thanked for their contributions to SOCAT. Float data were collected and made  
 freely available by the Southern Ocean Carbon and Climate Observations and Modeling (SOCCOM)  
 Project funded by the National Science Foundation, Division of Polar Programs (NSF PLR-1425989),  
 475 supplemented by NASA, and by the International Argo Program and the NOAA programs that contribute  
 to it. (<http://www.argo.ucsd.edu>, <http://argo.jcommops.org>). The Argo Program is part of the Global Ocean  
 Observing System.

480

## References

Bakker, D. C. E., Pfeil, B. Landa, C. S., Metzl, N., O'Brien, K. M., Olsen, A., Smith, K., Cosca, C.,  
 Harasawa, S., Jones, S. D., Nakaoka, S., Nojiri, Y., Schuster, U., Steinhoff, T., Sweeney, C., Takahashi, T.,  
 Tilbrook, B., Wada, C., Wanninkhof, R., Alin, S. R., Balestrini, C. F., Barbero, L., Bates, N. R., Bianchi,  
 485 A. A., Bonou, F., Boutin, J., Bozec, Y., Burger, E. F., Cai, W.-J., Castle, R. D., Chen, L., Chierici, M.,  
 Currie, K., Evans, W., Featherstone, C., Feely, R. A., Fransson, A., Goyet, C., Greenwood, N., Gregor, L.,  
 Hankin, S., Hardman-Mountford, N. J., Harlay, J., Hauck, J., Hoppema, M., Humphreys, M. P., Hunt, C.  
 W., Huss, B., Ibáñez, J. S. P., Johannessen, T., Keeling, R., Kitidis, V., Körtzinger, A., Kozyr, A.,  
 Krasakopoulou, E., Kuwata, A., Landschützer, P., Lauvset, S. K., Lefèvre, N., Lo Monaco, C., Manke, A.,  
 490 Mathis, J. T., Merlivat, L., Millero, F. J., Monteiro, P. M. S., Munro, D. R., Murata, A., Newberger, T.,  
 Omar, A. M., Ono, T., Paterson, K., Pearce, D., Pierrot, D., Robbins, L. L., Saito, S., Salisbury, J.,  
 Schlitzer, R., Schneider, B., Schweitzer, R., Sieger, R., Skjelvan, I., Sullivan, K. F., Sutherland, S. C.,  
 Sutton, A. J., Tadokoro, K., Telszewski, M., Tuma, M., Van Heuven, S. M. A. C., Vandemark, D., Ward,  
 B., Watson, A. J., Xu, S. (2016) A multi-decade record of high quality fCO<sub>2</sub> data in version 3 of the  
 495 Surface Ocean CO<sub>2</sub> Atlas (SOCAT). *Earth System Science Data* 8: 383-413. doi:10.5194/essd-8-383-2016.

Carter, B. R., Williams, N. L., Gray, A. R., & Feely, R. A. (2016). Locally interpolated alkalinity  
 regression for global alkalinity estimation. *Limnology and Oceanography: Methods*, 14(4), 268-277.

500 Ciais, P., and C. Sabine (2013), Chapter 6: Carbon and other biogeochemical cycles, in *Climate Change  
 2013: The Physical Science Basis. Contribution of Working Group I to the Fifth Assessment Report of the  
 Intergovernmental Panel on Climate Change*, edited by T. F. Stocker et al., p. 1535, Cambridge Univ.  
 Press, Cambridge, U. K., and New York.

Dlugokencky, E.J., K.A. Masarie, P.M. Lang, and P.P. Tans (2015), NOAA Greenhouse Gas Reference  
 from Atmospheric Carbon Dioxide Dry Air Mole Fractions from the NOAA ESRL Carbon Cycle



- 505 Cooperative Global Air Sampling Network. Data Path:  
[ftp://aftp.cmdl.noaa.gov/data/trace\\_gases/co2/flask/surface/](ftp://aftp.cmdl.noaa.gov/data/trace_gases/co2/flask/surface/).
- Dlugokencky, E. and P. Tans, 2017. NOAA/ESRL, [www.esrl.noaa.gov/gmd/ccgg/trends/](http://www.esrl.noaa.gov/gmd/ccgg/trends/) (accessed September 15, 2017).
- 510 Eveleth, R., Cassar, N., Doney, S. C., Munro, D. R., & Sweeney, C. (2017). Biological and physical controls on O<sub>2</sub>/Ar, Ar and pCO<sub>2</sub> variability at the Western Antarctic Peninsula and in the Drake Passage. *Deep Sea Research Part II: Topical Studies in Oceanography*, 139, 77-88.
- 515 Fay, A. R., & McKinley, G. A. (2013). Global trends in surface ocean pCO<sub>2</sub> from in situ data. *Global Biogeochemical Cycles*, 27(2), 541-557.
- Fay, A. R., and G. A. McKinley (2014), Global open-ocean biomes: Mean and temporal variability, *Earth Syst. Sci. Data*, 6(2), 273–284, doi:10.5194/essd-6-273-2014.
- 520 Fay, A. R., McKinley, G. A., & Lovenduski, N. S. (2014). Southern Ocean carbon trends: Sensitivity to methods. *Geophysical Research Letters*, 41(19), 6833-6840.
- Freeman, N.M., and N.S. Lovenduski, (2016) Mapping the Antarctic Polar Front: weekly realizations from 2002 to 2014, *Earth System Science Data*, 8, 191-198, doi:10.5194/essd-8-191-2016.
- 525 Freeman, N.M., N.S. Lovenduski, and P.R. Gent, (2016) Temporal variability in the Antarctic Polar Front (2001-2014), *Journal of Geophysical Research: Oceans*, 121, 7263-7276, doi:10.1002/2016JC012145.
- Frölicher, T. L., Sarmiento, J. L., Paynter, D. J., Dunne, J. P., Krasting, J. P., & Winton, M. (2015). Dominance of the Southern Ocean in anthropogenic carbon and heat uptake in CMIP5 models. *Journal of Climate*, 28(2), 862-886.
- 530 Gruber et al. 2009: Gruber, N., Gloor, M., Mikaloff Fletcher, S. E., Doney, S. C., Dutkiewicz, S., Follows, M. J., Gerber, M., Jacobson, A. R., Joos, F., Lindsay, K., Menemenlis, D., Mouchet, A., Müller, S. A., Sarmiento, J. L., and Takahashi, T. (2009) Oceanic sources, sinks, and transport of atmospheric CO<sub>2</sub>, *Global Biogeochem. Cy.*, 23, GB1005, doi:10.1029/2008GB003349.
- 535 Hoppema, M., Velo, A., Heuven, S. V., Tanhua, T., Key, R. M., Lin, X., Sabine, C. L. (2009). Consistency of cruise data of the CARINA database in the Atlantic sector of the Southern Ocean. *Earth System Science Data*, 1(1), 63-75.
- 540 Johnson, K.S., Jannasch, H.W., Coletti, L.J., Elrod, V.A., Martz, T.R., Takeshita, Y., Carlson, R.J. and Connery, J.G. (2016) Deep-Sea DuraFET: A pressure tolerant pH sensor designed for global sensor networks. *Analytical Chemistry*, 88(6), pp.3249-3256.
- 545 Johnson, K. S., Plant, J. N., Coletti, L. J., Jannasch, H. W., Sakamoto, C. M., Riser, S. C., Talley, L. D. (2017) Biogeochemical sensor performance in the SOCCOM profiling float array. *Journal of Geophysical Research: Oceans* doi:10.1002/2017JC012838.
- 550 Landschützer, P., N. Gruber, D. C. E. Bakker, and U. Schuster (2014a), Recent variability of the global ocean carbon sink, *Global Biogeochem. Cycles*, 28, 927–949, doi:10.1002/2014GB004853.
- Landschützer, P., Gruber, N., Bakker, D. C. E., Schuster, U. (2014b) An observation-based global monthly gridded sea surface pCO<sub>2</sub> product from 1998 through 2011 and its monthly climatology, available on: [http://cdiac.ornl.gov/oceans/SPCO2\\_1998\\_2011\\_ETH\\_SOM\\_FFN.html](http://cdiac.ornl.gov/oceans/SPCO2_1998_2011_ETH_SOM_FFN.html).
- 555 Landschützer, P., Gruber, N., Haumann, F., Rödenbeck, C., Bakker, D., van Heuven, S., Hoppema, M., Metz, N., Sweeney, C., Taka-hashi, T., Tilbrook, B., and Wanninkhof, R. (2015a) The reinvigoration of



the Southern Ocean carbon sink, *Science*, 349, 1221–1224.

- 560 Landschützer, P., N. Gruber, and D.C.E. Bakker. (2015b). A 30 years observation-based global monthly gridded sea surface pCO<sub>2</sub> product from 1982 through 2011. [http://cdiac.ornl.gov/ftp/oceans/SPCO2\\_1982\\_2011\\_ETH\\_SOM\\_FFN](http://cdiac.ornl.gov/ftp/oceans/SPCO2_1982_2011_ETH_SOM_FFN). Carbon Dioxide Information Analysis Center, Oak Ridge National Laboratory, US Department of Energy, Oak Ridge, Tennessee. doi: 10.3334/CDIAC/OTG.SPCO2\_1982\_2011\_ETH\_SOM-FFN
- 565 Landschützer, P., Gruber, N., Bakker, D. C. E. (2016) Decadal variations and trends of the global ocean carbon sink, *Global Biogeochemical Cycles*, 30, doi:10.1002/2015GB005359
- 570 Landschützer, P., Gruber, N., Bakker, D. C. E. (2017). An updated observation-based global monthly gridded sea surface pCO<sub>2</sub> and air-sea CO<sub>2</sub> flux product from 1982 through 2015 and its monthly climatology (NCEI Accession 0160558). Version 2.2. NOAA National Centers for Environmental Information. Dataset. [2017-07-11]: available at [https://www.nodc.noaa.gov/ocads/oceans/SPCO2\\_1982\\_2015\\_ETH\\_SOM\\_FFN.html](https://www.nodc.noaa.gov/ocads/oceans/SPCO2_1982_2015_ETH_SOM_FFN.html)
- 575 Le Quéré, C., Rödenbeck, C., Buitenhuis, E. T., Conway, T. J., Langenfelds, R., Gomez, A., Labuschagne, C., Ramonet, M., Nakazawa, T., Metzl, N., Gillett, N., and Heimann, M. (2007) Saturation of the Southern Ocean CO<sub>2</sub> sink due to recent climate change, *Science*, 316, 1735–1738, doi:10.1126/science.1136188.
- 580 Le Quéré, C., Robbie M. Andrew, Josep G. Canadell, Stephen Sitch, Jan Ivar Korsbakken, Glen P. Peters, Andrew C. Manning, Thomas A. Boden, Pieter P. Tans, Richard A. Houghton, Ralph F. Keeling, Simone Alin, Oliver D. Andrews, Peter Anthoni, Leticia Barbero, Laurent Bopp, Frédéric Chevallier, Louise P. Chini, Philippe Ciais, Kim Currie, Christine Delire, Scott C. Doney, Pierre Friedlingstein, Thanos Gkritzalis, Ian Harris, Judith Hauck, Vanessa Haverd, Mario Hoppema, Kees Klein Goldewijk, Atul K. Jain, Etsushi Kato, Arne Körtzinger, Peter Landschützer, Nathalie Lefèvre, Andrew Lenton, Sebastian Lienert, Danica Lombardozi, Joe R. Melton, Nicolas Metzl, Frank Millero, Pedro M. S. Monteiro, David R. Munro, Julia E. M. S. Nabel, Shin-ichiro Nakaoka, Kevin O'Brien, Are Olsen, Abdurahman M. Omar, Tsuneo Ono, Denis Pierrot, Benjamin Poulter, Christian Rödenbeck, Joe Salisbury, Ute Schuster, Jörg Schwinger, Roland Séférian, Ingunn Skjelvan, Benjamin D. Stocker, Adrienne J. Sutton, Taro Takahashi, Hanqin Tian, Bronte Tilbrook, Ingrid T. van der Laan-Luijkx, Guido R. van der Werf, Nicolas Viovy, Anthony P. Walker, Andrew J. Wiltshire, Sönke Zaehle (2016), *Earth System Science Data*, DOI:10.5194/essd-8-605-2016.
- 585
- 590 Le Quéré, C., Andrew, R. M., Friedlingstein, P., Sitch, S., Pongratz, J., Manning, A. C., Korsbakken, J. I., Peters, G. P., Canadell, J. G., Jackson, R. B., Boden, T. A., Tans, P. P., Andrews, O. D., Arora, V. K., Bakker, D. C. E., Barbero, L., Becker, M., Betts, R. A., Bopp, L., Chevallier, F., Chini, L. P., Ciais, P., Cosca, C. E., Cross, J., Currie, K., Gasser, T., Harris, I., Hauck, J., Haverd, V., Houghton, R. A., Hunt, C. W., Hurtt, G., Ilyina, T., Jain, A. K., Kato, E., Kautz, M., Keeling, R. F., Klein Goldewijk, K., Körtzinger, A., Landschützer, P., Lefèvre, N., Lenton, A., Lienert, S., Lima, I., Lombardozi, D., Metzl, N., Millero, F., 595 Monteiro, P. M. S., Munro, D. R., Nabel, J. E. M. S., Nakaoka, S.-I., Nojiri, Y., Padín, X. A., Pregon, A., Pfeil, B., Pierrot, D., Poulter, B., Rehder, G., Reimer, J., Rödenbeck, C., Schwinger, J., Séférian, R., Skjelvan, I., Stocker, B. D., Tian, H., Tilbrook, B., van der Laan-Luijkx, I. T., van der Werf, G. R., van Heuven, S., Viovy, N., Vuichard, N., Walker, A. P., Watson, A. J., Wiltshire, A. J., Zaehle, S., and Zhu, D. 600 (2017) Global Carbon Budget 2017, *Earth Syst. Sci. Data Discuss.*, <https://doi.org/10.5194/essd-2017-123>, in review.
- 605 Lo Monaco, C., Metzl, N., Poisson, A., Brunet, C., & Schauer, B. (2005). Anthropogenic CO<sub>2</sub> in the Southern Ocean: Distribution and inventory at the Indian-Atlantic boundary (World Ocean Circulation Experiment line I6). *Journal of Geophysical Research: Oceans*, 110(C6).
- Lo Monaco, C. L., Alvarez, M., Key, R. M., Lin, X., Tanhua, T., Tilbrook, B., Ríos, A. F. (2010). Assessing the internal consistency of the CARINA database in the Indian sector of the Southern Ocean. *Earth System Science Data*, 2(1), 51.



- 610 Lovenduski, N. S., Gruber, N., & Doney, S. C. (2008). Toward a mechanistic understanding of the decadal trends in the Southern Ocean carbon sink. *Global Biogeochemical Cycles*, 22(3).
- 615 Lovenduski, N. S., A. R. Fay, and G. A. McKinley (2015), Observing multidecadal trends in Southern Ocean CO<sub>2</sub> uptake: What can we learn from an ocean model?, *Global Biogeochem. Cycles*, 29(4), 416–426, doi:10.1002/2014GB004933.
- 620 Majkut, J. D., Carter, B. R., Frölicher, T. L., Dufour, C. O., Rodgers, K. B., & Sarmiento, J. L. (2014). An observing system simulation for Southern Ocean carbon dioxide uptake. *Phil. Trans. R. Soc. A*, 372(2019), 20130046.
- 625 McKinley, G. A., Fay, A. R., Lovenduski, N. S., & Pilcher, D. J. (2017). Natural variability and anthropogenic trends in the ocean carbon sink. *Annual review of marine science*, 9, 125-150.
- Metzl, N., Tilbrook, B., & Poisson, A. (1999). The annual fCO<sub>2</sub> cycle and the air-sea CO<sub>2</sub> flux in the sub-Antarctic Ocean. *Tellus B: Chemical and Physical Meteorology*, 51(4), 849-861.
- Metzl, N. (2009). Decadal increase of oceanic carbon dioxide in Southern Indian Ocean surface waters (1991–2007). *Deep Sea Research Part II: Topical Studies in Oceanography*, 56(8), 607-619.
- 630 Munro, D. R., N. S. Lovenduski, T. Takahashi, B. B. Stephens, T. Newberger, and C. Sweeney (2015a), Recent evidence for a strengthening CO<sub>2</sub> sink in the Southern Ocean from carbonate system measurements in the Drake Passage (2002–2015), *Geophys. Res. Lett.*, 42, 7623–7630, doi:10.1002/2015GL065194.
- 635 Munro, D. R., et al. (2015b), Estimates of net community production in the Southern Ocean determined from time series observations (2002–2011) of nutrients, dissolved inorganic carbon, and surface ocean pCO<sub>2</sub> in Drake Passage, *Deep Sea Res., Part II*, 114, 49–63, doi:10.1016/j.dsr2.2014.12.014.
- Olsen, A., N. Metzl, D. Bakker, K. O'Brien (2013), SOCAT QC cookbook for SOCAT participants; available at: [https://www.socat.info/wp-content/uploads/2017/04/2015\\_SOCAT\\_QC\\_Cookbook\\_v3.pdf](https://www.socat.info/wp-content/uploads/2017/04/2015_SOCAT_QC_Cookbook_v3.pdf), last access: 01 November 2017.
- 640 Pfeil, B., Olsen, A., Bakker, D. C. E., Hankin, S., Koyuk, H., Kozyr, A., Malczyk, J., Manke, A., Metzl, N., Sabine, C. L., Akl, J., Alin, S. R., Bates, N., Bellerby, R. G. J., Borges, A., Boutin, J., Brown, P. J., Cai, W.-J., Chavez, F. P., Chen, A., Cosca, C., Fassbender, A. J., Feely, R. A., González-Dávila, M., Goyet, C., Hales, B., Hardman-Mountford, N., Heinze, C., Hood, M., Hoppema, M., Hunt, C. W., Hydes, D., Ishii, M., Johannessen, T., Jones, S. D., Key, R. M., Körtzinger, A., Landschützer, P., Lauvset, S. K., Lefèvre, N., Lenton, A., Lourantou, A., Merlivat, L., Midorikawa, T., Mintrop, L., Miyazaki, C., Murata, A., Nakadate, A., Nakano, Y., Nakaoka, S., Nojiri, Y., Omar, A. M., Padin, X. A., Park, G.-H., Paterson, K., Perez, F. F., Pierrot, D., Poisson, A., Rios, A. F., Santana-Casiano, J. M., Salisburly, J., Sarma, V. V. S. S., Schlitzer, R., Schneider, B., Schuster, U., Sieger, R., Skjelvan, I., Steinhoff, T., Suzuki, T., Takahashi, T., Tedesco, K., Telszewski, M., Thomas, H., Tilbrook, B., Tjiputra, J., Vandemark, D., Veness, T., Wanninkhof, R., Watson, A. J., Weiss, R., Wong, C. S., Yoshikawa-Inoue, H. (2013) A uniform, quality controlled Surface Ocean CO<sub>2</sub> Atlas (SOCAT), *Earth System Science Data* 5: 125-143. doi:10.5194/essd-5-125-2013.
- 650 655 Rödenbeck, C., Bakker, D. C., Gruber, N., Iida, Y., Jacobson, A. R., Jones, S., Park, G. H. (2015). Data-based estimates of the ocean carbon sink variability—first results of the Surface Ocean pCO<sub>2</sub> Mapping intercomparison (SOCOM). *Biogeosciences*, 12, 7251-7278.
- 660 Sabine, C.L., Hankin, S., Koyuk, H., Bakker, D. C. E., Pfeil, B., Olsen, A., Metzl, N., Kozyr, A., Fassbender, A., Manke, A., Malczyk, J., Akl, J., Alin, S. R., Bellerby, R. G. J., Borges, A., Boutin, J., Brown, P. J., Cai, W.-J., Chavez, F. P., Chen, A., Cosca, C., Feely, R. A., González-Dávila, M., Goyet, C., Hardman-Mountford, N., Heinze, C., Hoppema, M., Hunt, C. W., Hydes, D., Ishii, M., Johannessen, T.,



- 665 Key, R. M., Körtzinger, A., Landschützer, P., Lauvset, S. K., Lefèvre, N., Lenton, A., Lourantou, A., Merlivat, L., Midorikawa, T., Mintrop, L., Miyazaki, C., Murata, A., Nakadate, A., Nakano, Y., Nakaoka, S., Nojiri, Y., Omar, A. M., Padin, X. A., Park, G.-H., Paterson, K., Perez, F. F., Pierrot, D., Poisson, A., Rios, A. F., Salisbury, J., Santana-Casiano, J. M., Sarma, V. V. S. S., Schlitzer, R., Schneider, B., Schuster, U., Sieger, R., Skjelvan, I., Steinhoff, T., Suzuki, T., Takahashi, T., Tedesco, K., Telszewski, M., Thomas, H., Tilbrook, B., Vandemark, D., Veness, T., Watson, A. J., Weiss, R., Wong, C. S., Yoshikawa-Inoue, H. (2013) Surface Ocean CO<sub>2</sub> Atlas (SOCAT) gridded data products. *Earth System Science Data* 5: 145-153. doi:10.5194/essd-5-145-2013.
- 670 Shadwick, E. H., Trull, T. W., Tilbrook, B., Sutton, A. J., Schulz, E., & Sabine, C. L. (2015). Seasonality of biological and physical controls on surface ocean CO<sub>2</sub> from hourly observations at the Southern Ocean Time Series site south of Australia. *Global Biogeochemical Cycles*, 29(2), 223-238.
- 675 Sprintall, J., Chereskin, T. K., & Sweeney, C. (2012). High-resolution underway upper ocean and surface atmospheric observations in Drake Passage: Synergistic measurements for climate science. *Oceanography*, 25(3), 70-81.
- 680 Takahashi, T., Sutherland, S. C., Sweeney, C., Poisson, A., Metzl, N., Tilbrook, B., Bates, N., Wanninkhof, R., Feely, R. F., Sabine, C., Olafsson, J., and Nojiri, Y. (2002) Global sea-air CO<sub>2</sub> flux based on climatological surface ocean pCO<sub>2</sub> and seasonal biological and temperature effects, *Deep-Sea Res. Pt. II*, 49, 1601–1622.
- 685 Takahashi, T., Sutherland, S., Wanninkhof, R., Sweeney, C., Feely, R., Chipman, D., Hales, B., Friederich, G., Chavez, F., Sabine, C., Watson, A., Bakker, D., Schuster, U., Metzl, N., Yoshikawa-Inoue, H., Ishii, M., Midorikawa, T., Nojiri, Y., Körtzinger, A., Steinhoff, T., Hoppema, M., Olafson, J., Arnarson, T., Tilbrook, B., Johannessen, T., Olsen, A., Bellerby, R., Wong, C., Delille, B., Bates, N., and de Baar, H. (2009) Climatological mean and decadal change in surface ocean pCO<sub>2</sub>, and net sea-air CO<sub>2</sub> flux over the global oceans, *Deep-Sea Res. Pt. II*, 56, 554–577.
- 690 Takahashi, T., Sweeney, C., Hales, B., Chipman, D. W., Newberger, T., Goddard, J. G., Iannuzzi, R.A., & Sutherland, S. C. (2012). The changing carbon cycle in the Southern Ocean. *Oceanography*, 25(3), 26-37.
- 695 van Heuven, S. M., Hoppema, M., Huhn, O., Slagter, H. A., & de Baar, H. J. (2011). Direct observation of increasing CO<sub>2</sub> in the Weddell Gyre along the Prime Meridian during 1973–2008. *Deep Sea Research Part II: Topical Studies in Oceanography*, 58(25), 2613-2635.
- 700 Williams, N. L., Juranek, L. W., Johnson, K. S., Feely, R. A., Riser, S. C., Talley, L. D., Russell, J.L., Sarmiento, J.L., & Wanninkhof, R. (2016). Empirical algorithms to estimate water column pH in the Southern Ocean. *Geophysical Research Letters*, 43(7), 3415-3422.
- 705 Williams et al. 2017: Williams, N. L., Juranek, L. W., Feely, R. A., Johnson, K. S., Sarmiento, J. L., Talley, L. D., Riser, S. C. (2017). Calculating surface ocean pCO<sub>2</sub> from biogeochemical Argo floats equipped with pH: an uncertainty analysis. *Global Biogeochemical Cycles*, 31(3), 591-604.
- 710 Xue, L., Gao, L., Cai, W. J., Yu, W., & Wei, M. (2015). Response of sea surface fugacity of CO<sub>2</sub> to the SAM shift south of Tasmania: Regional differences. *Geophysical Research Letters*, 42(10), 3973-3979.
- 715



#### Figure Captions

##### Figure 1

Map of Fay and McKinley [2014] biomes that are defined at  $1^\circ \times 1^\circ$  resolution. Subpolar seasonally stratified (SPSS) biome shown in teal. The red line represents the mean location of the Antarctic Polar Front [Freeman and Lovenduski, 2016], interpolated to a  $1^\circ \times 1^\circ$  grid. The black box represents the Drake Passage region considered in this analysis.

##### Figure 2

Mean surface ocean  $p\text{CO}_2$  seasonal cycle estimate for years 2002-2015, for the SPSS biome from each dataset, shown on an 18-month cycle, calculated from a time-series with the atmospheric trend removed ( $1.95 \mu\text{atm yr}^{-1}$ ). Shading represents 1 standard error for biome-scale monthly means. Bar plot indicates the number of years containing observations in a given month (maximum of 14 years) for the SOCAT-DP, SOCAT-noDP, and SOCAT-all datasets.

730

##### Figure 3

Data density of  $p\text{CO}_2$  observations from the SOCATv4 dataset within each  $1^\circ \times 1^\circ$  gridcell. Data is restricted to years 2002-2015. Salinity values outside of 33.5-34.5 psu and observations within 50 km of land are omitted. (a) data from all months of the year; (b) data from only June, July, and August (austral winter).

735

##### Figure 4

(a) Temporal evolution of deseasonalized, detrended monthly SOCAT-DP  $p\text{CO}_2$  anomalies (gray bars) over 2002-2015, with 12-month running averages (black line) overlain. (b) Correlation between monthly SOCAT-DP  $p\text{CO}_2$  anomalies and the  $p\text{CO}_2$  anomalies estimated from the SOM-FFN-noDP product (created without the inclusion of Drake Passage data), for years 2002-2015 at each  $1^\circ \times 1^\circ$  grid cell. Gray shading represents areas where the correlation does not pass significance t-tests at  $p < 0.05$ .

740

##### Figure 5



Surface ocean pCO<sub>2</sub> trends in the SPSS biome for years 2002-2015 ( $\mu\text{atm yr}^{-1}$ ): SOCATv4 data within the  
745 Drake Passage box (gray); SOCATv4 data excluding data from the Drake Passage box (green); SOCATv4  
(blue); SOM-FFN product (magenta); SOM-FFN pCO<sub>2</sub> product sampled as SOCATv4 data in the Drake  
Passage box (light pink). Figure includes annual trends (left), summer trends (center) and winter trends  
(right). SOCAT-noDP winter trend omitted because it did not contain a JJA value for every year of the  
time-series. For reference, the atmospheric pCO<sub>2</sub> trend during the 2002-2015 period ( $1.95 \mu\text{atm yr}^{-1}$ ) is  
750 shown as a horizontal black line.

#### Figure 6

(a) Sea-air CO<sub>2</sub> flux and (b) pCO<sub>2</sub> averaged over the Southern Ocean (south of 35°S) from the SOM-FFN  
pCO<sub>2</sub> product (blue) and that of the SOM-FFN-noDP product created without the inclusion of Drake  
755 Passage data (red). Trends and uncertainty values in corresponding colors.

#### Figure 7

(a) 2002-2017 underway DPT pCO<sub>2</sub> observations (circles) and surface pCO<sub>2</sub> estimates from SOCCOM  
floats overlain (diamonds;  $\mu\text{atm}$ ), plotted versus latitude. (b) Trajectories of Drake Passage-transiting  
760 SOCCOM floats included in this analysis. Colored dots represent the location of surface measurements for  
each float. Data from floats collected east of 55°W and west of 90°W are not included in this analysis. Gray  
dots represent observations from the DPT. (c) Same as (a) but plotted as October 2015 to September 2017.

#### Figure 8

765 (a) Map of SOCCOM floats with DPT crossovers within 75km, 3 days, and 0.3°C SST from coincident  
surface observations. (b) Calculated pCO<sub>2</sub> from SOCCOM float (x-axis) versus DPT underway pCO<sub>2</sub>  
observations (y-axis) for crossover float locations, with 1:1 line. Colors correspond to float number in  
Figure 7. Horizontal width of shading represents SOCCOM relative standard uncertainty which is  
estimated at  $11 \mu\text{atm}$ ; vertical shading is  $2 \mu\text{atm}$  uncertainty around DPT observations. Black 'x' and  
770 squares indicated crossovers within a smaller window (50km/2day/0.3°C SST and 25km/1day/0.3°C SST  
respectively).

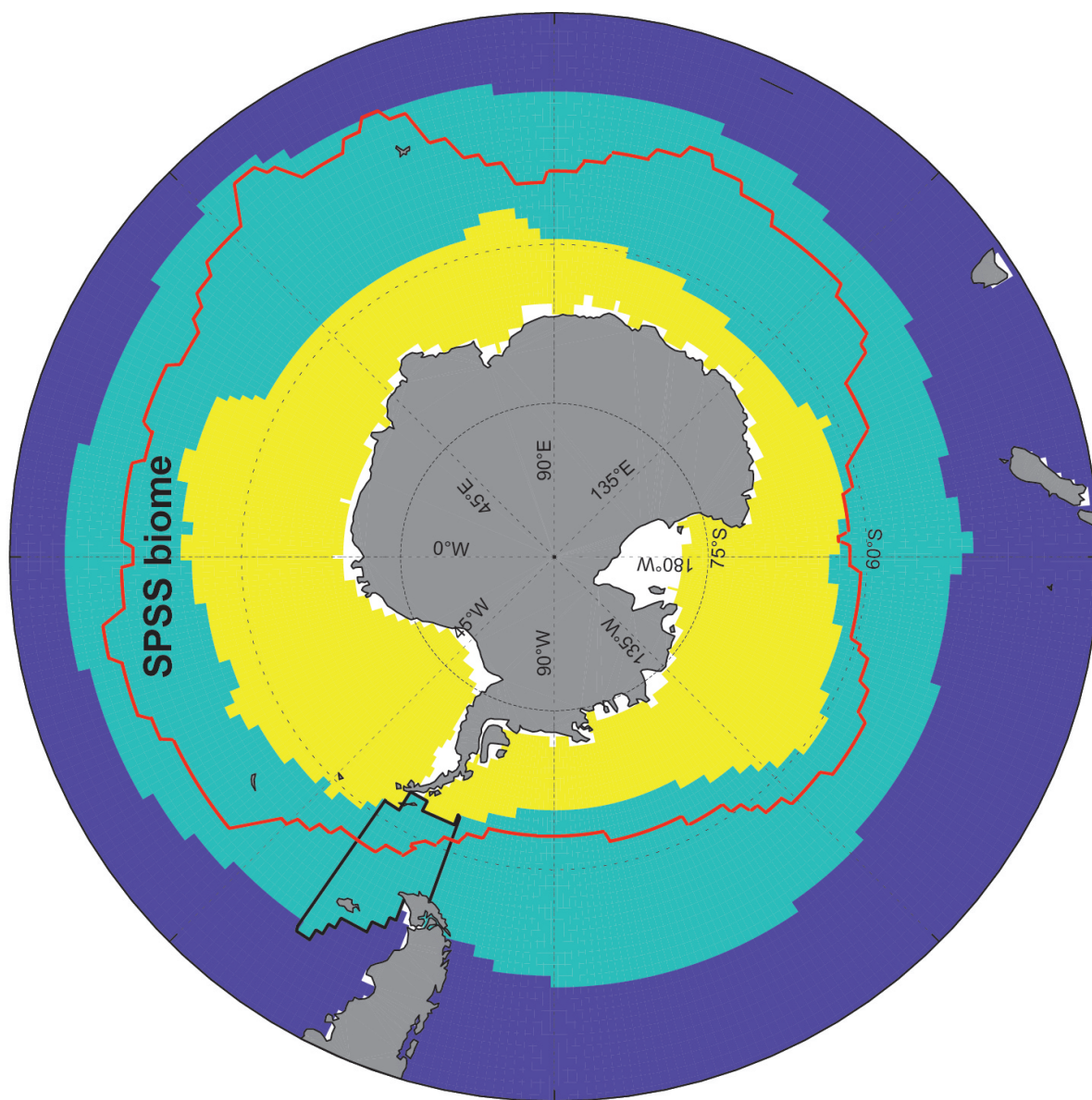
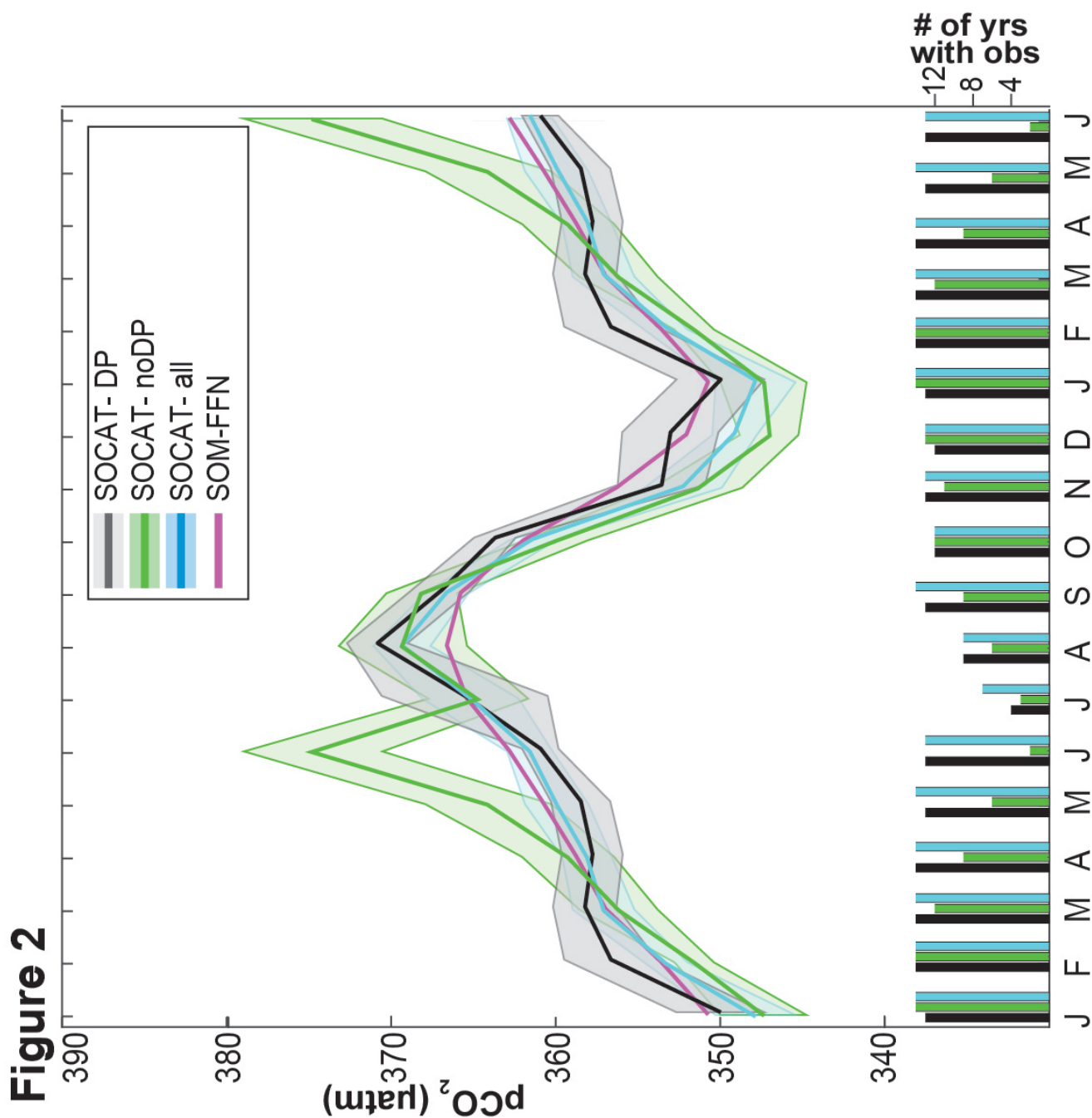


Figure 1



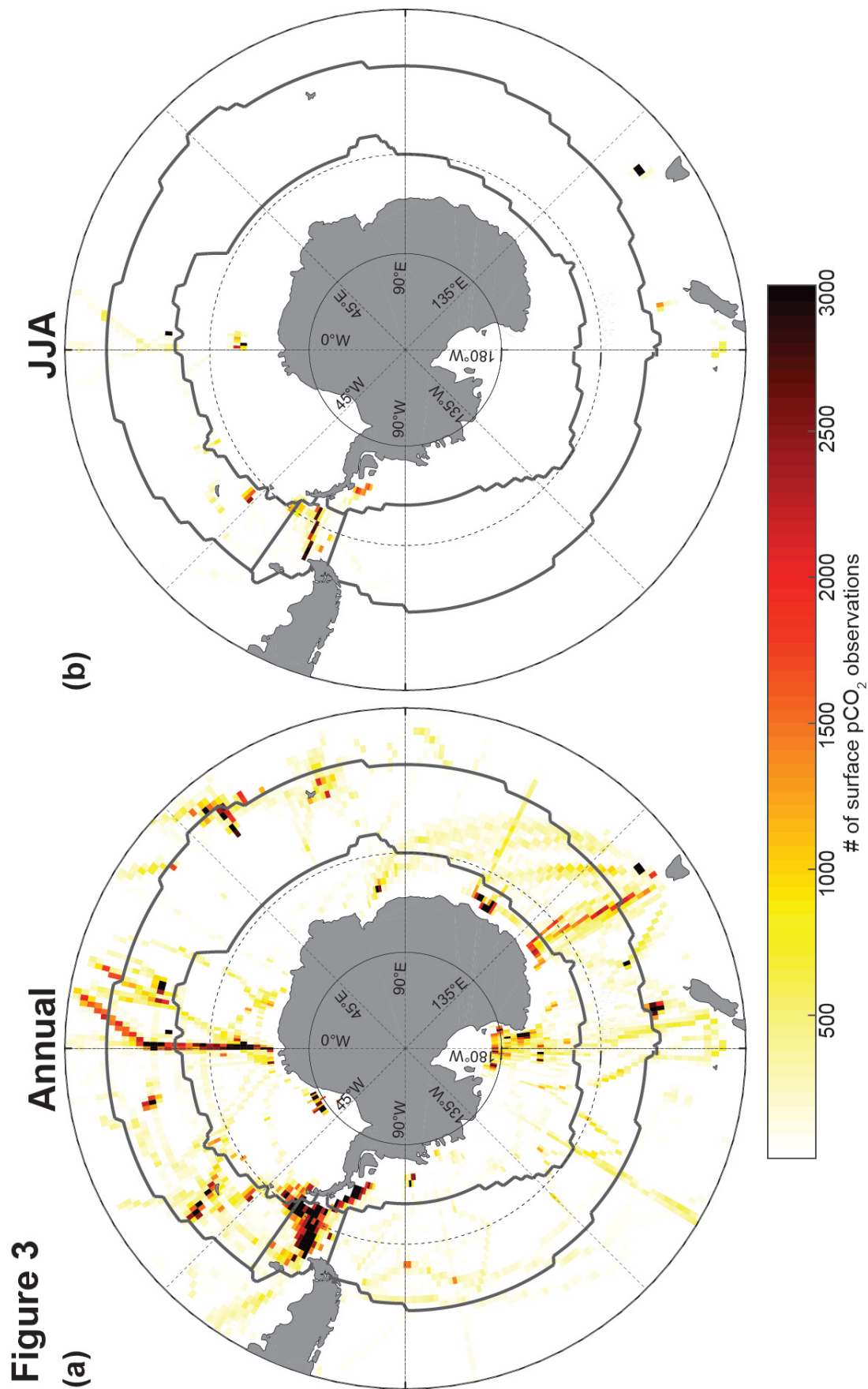


Figure 3

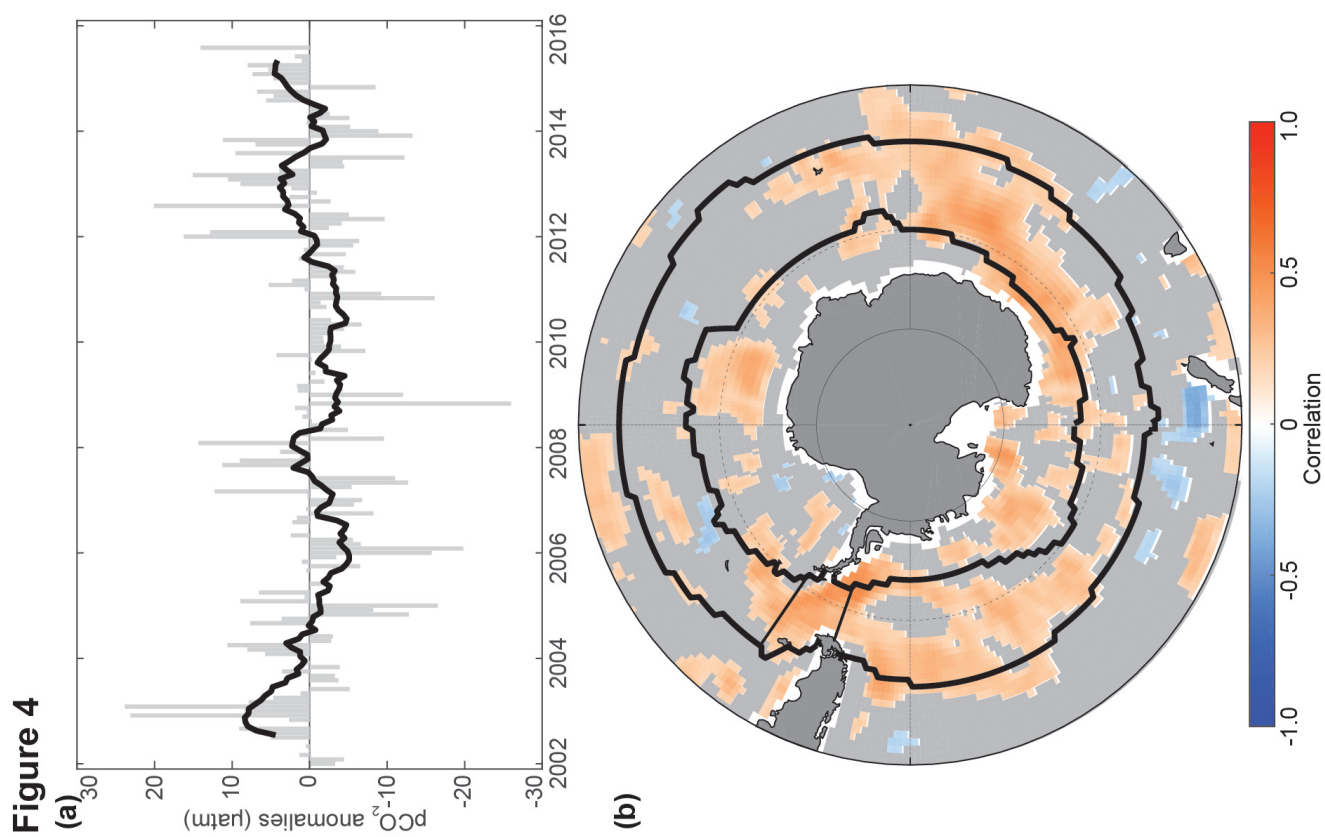




Figure 5

